# Controlling the geometry of laser ablated microneedle cavities in different mould materials and assessing the replication fidelity within polymer injection moulding

# Controlling the geometry of laser ablated microneedle cavities in different mould materials and assessing the replication fidelity within polymer injection moulding

Tim Evens[1], Olivier Malek[2], Sylvie Castagne[3], David Seveno[4], Albert Van Bael[1,4]

[1] KU Leuven, Department of Materials Engineering Diepenbeek Campus, Wetenschapspark 27, 3590 Diepenbeek, Belgium

[2] Sirris, Precision Manufacturing, Wetenschapspark 9, 3590 Diepenbeek, Belgium

[3] KU Leuven, Department of Mechanical Engineering and Flanders Make@KU Leuven-MaPS, Celestijnenlaan 300, 3001 Leuven, Belgium

[4] KU Leuven, Department of Materials Engineering, Kasteelpark Arenberg 44, 3001 Leuven, Belgium

*Correspondence to: Tim Evens (E-mail: tim.evens@kuleuven.be)*

**ABSTRACT**

Microneedle arrays are minimally invasive devices which enable self-administration of drugs in a straightforward and efficient way. Recently, a low-cost mass production method to produce solid polymer microneedles using laser ablated moulds in an injection moulding process has been developed. In this context, it is key to understand how the geometry of the microneedle cavities can be changed and what parameters affect the replication fidelity during injection moulding. In this study, two laser scanning parameters, being the programmed base diameter and the number of layers were varied in four levels and their effects on the geometry of the microneedle cavities were evaluated in tool steel, copper alloy, and aluminium alloy inserts. Afterwards, the microneedle cavities were replicated in polypropylene and polycarbonate using injection moulding. The study showed how the depth and base diameter of the microneedle cavity can be changed by varying laser scanning parameters. Moreover, the moulds in the three materials exhibited different microneedle cavity shapes and dimensions, due to differences in material properties. As to the injection moulding process, strong linear relationships were found between the aspect ratio of the microneedle cavities and the replicated thermoplastic microneedles, where a higher aspect ratio resulted in a lower replication. The replication fidelity for the polypropylene microneedles was in all cases higher compared to the polycarbonate needles. Between the three mould materials, a comparable replication fidelity was found for tool steel and copper alloy and a lower replication for the aluminium alloy, due to differences in thermal and wetting properties.

**KEYWORDS**

Laser machining; Injection Moulding; Microneedles; Micro manufacturing

## 1. INTRODUCTION

Traditional needles, known as hypodermic needles, are used in clinical practice to sample blood or to deliver vaccines or medication across the skin into the blood stream [1]. Although such needles are very frequently used, they are known to induce discomfort to the patient, like pain or bruising and carry the risk of infections. Besides, the use of these systems requires trained medical staff. A possible alternative to the hypodermic needles are microneedles. These are microscale invasive devices, usually arranged in an array and designed to by-pass the human stratum corneum skin barrier [2,3]. The length of the needles ranges from 25 µm – 2500 µm and when penetrated in the skin, they can deliver vaccines, antibodies or other drugs to the human body through the transdermal route [4]. These systems offer various advantages such as (i) a pain free drug delivery, (ii) self-administration, (iii) lower storage, distribution and disposal cost due to the small volume, and (iv) direct administration of vaccines to key immune cells [5–7].

The first concept using microneedles for vaccine delivery was conceived by Alza corporation, as described in a 1976 patent [5]. Making these devices was not possible until the 1990s, when the technology needed to fabricate micrometre sized structures became available. Since then, many researches both from academia and industry have demonstrated the applicability of microneedle devices, from the development phase up to clinical experiments. The investigated methods for manufacturing these microscale devices covers a wide range of techniques such as, chemical etching [8], polymer replication techniques [9–11], additive manufacturing [12], surface micromachining [13], and photolithography [14]. According to World Health Organization guidelines, cost-effective, portable, disposable medical devices are needed in order to enhance the health-related quality of life worldwide [16]. Yet, for most of the current manufacturing methods the low cost and high volumes still pose a great challenge [15]. Polymer injection moulding has a huge potential, as this manufacturing process has already proven to be very suitable to manufacture polymer medical devices, due to its high accuracy, potential for full-automation, short cycle times, and low cost. Moreover, polymers can offer excellent biocompatibility, biodegradability, low toxicity, and good mechanical properties at a low material cost [17].

In a recent work [18], we demonstrated a novel methodology to mass produce solid polymer microneedles using laser ablated moulds in an injection moulding process. We were able to create solid cone-shaped microneedles with low tip radii < 20 µm. These needles can be used for drug delivery using two techniques. With the first technique, called 'poke with patch' approach (Figure 1a), the solid microneedles are used to pierce the skin, creating transient aqueous micro-pores through which a medical solution can passively diffuse. In the second approach, the solid needles are coated with a drug formulation (Figure 1b). After insertion, the coated drug formulation will be dissolved and deposited in the skin.

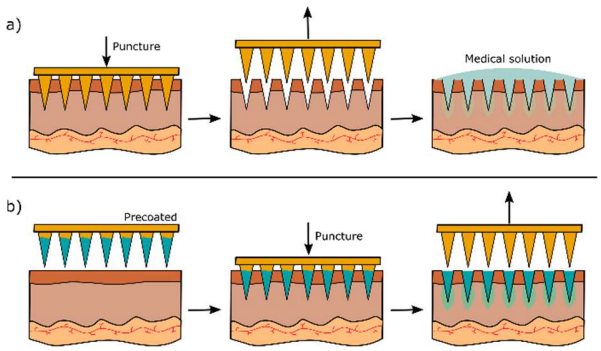


**Figure 1** A schematic representation of the different types of microneedles. (a) Solid microneedles (b) Coated microneedles. After [15].

The size of the needles depends on the specific medical application, while the design should allow for the needles to penetrate into the skin or any other biological tissue without breaking or bending. It is therefore important to know how to fine-tune the parameters in the manufacturing process to optimize the geometry of the microneedles. The manufacturing method combines laser ablation and injection moulding and these two processes will both affect the geometry of the needle.

In this study, we investigate the influence of two laser scanning parameters, being the programmed base diameter and the number of layers, on the geometry of microneedle cavities within a femtosecond laser ablation process. This evaluation is done for the three most common mould materials used in injection moulding, being tool steel, copper alloy, and aluminium alloy [19]. In addition, the replication fidelity of the laser induced cavities are evaluated using polymer injection moulding.

## 2. Materials and methods

### 2.1 *Thermoplastic and mould materials*

Two thermoplastic materials were used in this study: polypropylene (PP, 578N, manufactured by SABIC) and polycarbonate (PC, Lexan™ HPX8REU, manufactured by SABIC). The polypropylene material is a general purpose semi-crystalline homopolymer, which is easy to process and has a low cost. The polycarbonate material is a biocompatible amorphous grade, suitable for medical devices and pharmaceutical applications. Both materials have a high flowability as indicated by their very high melt volume rate (MVR) and are thus appropriate for filling small micro features. Table 1 reports the main characteristics for both thermoplastics.

**Table 1** Main properties of the thermoplastics based on material datasheets and Autodesk Moldflow® 2019 material database.

| | PP | PC |
|---|---|---|
| Density (kg/m³) | 928.9 | 1188.9 |
| Melt flow rate (g/10 min) | 245 [230 °C/2.16 kg] | 35 [300 °C/1.2 kg] |
| Tensile Modulus (MPa) | 2100 | 2360 |
| Thermal conductivity (W/m °C) | 0.171 | 0.267 |
| Specific heat (J/g °C) | 2.94 | 1.86 |
| No-flow temperature (°C) | 109 | 147 |

Three materials were selected as mould inserts: a low corrosion tool steel “Stavax” (grade 1.2083 - AISI 420), a high-strength aluminium zinc alloy (grade 3.4365), and a copper nickel alloy (grade AMPCOLOY® 940). Tool steel is most often used because of its high wear resistance, leading to a long lifetime. The aluminium material is regularly used for low production series and prototype moulds, due to its low cost and good machinability. The copper alloy exhibits a very high thermal conductivity which improves the cooling and can in turn, decrease the injection moulding cycle time [20]. Besides, this material currently acts as an excellent alternative for Beryllium copper alloys, as it avoids health risks [21]. The main properties of these three materials are listed in Table 2.

**Table 2** Main properties of the different mould materials based on material datasheets and GRANTA EduPack.

| | Tool steel 1.2083 | Copper AMPCOLOY 940 | Aluminium 3.4365 |
|---|---|---|---|
| Density (kg/m³) | 7700 | 8710 | 2800 |
| Thermal conductivity at 100°C (W/m °C) | 23.5 | 226 | 145 |
| Specific heat capacity at 100°C (J/g °C) | 0.48 | 0.38 | 0.95 |
| Thermal diffusivity (mm²/s) | 6.51 | 68.36 | 60.40 |

### *2.2 Laser machining experiments*

A micromachining system (Lasea LS5) with a femtosecond laser source (Satsuma HP, Amplitude Systemes) is employed to laser ablate the mould inserts with dimensions 70 mm x 60 mm x 4.4 mm. The laser source emits a beam with a pulse length of 250 fs, a wavelength of 1030 nm and a pulse repetition rate of 500 kHz. The laser has a power of 10W with a loss factor of 0.785, giving a deliverable pulse energy of 15.7 µJ. A galvanometer steers the laser beam within the focal plane, with a spot size diameter of 15.0 µm and a pulse fluence of 8.88 J/cm². The energy distribution of the beam is Gaussian shaped with a laser beam quality value of $M^2 < 1.2$. Small dust particles which are formed from ablating the metal surface are extracted by a vacuum collect unit. After the laser texturing operation, the inserts are ultra-sonicated in an ethanol bath for 15 min to remove debris from the micro-holes.

A cross-hatching strategy was used as presented in a previous study [18]. The laser spot scans a circular region and follows parallel lines in two perpendicular directions. The distance between two consecutive lines is defined as the hatch pitch. Once the laser has scanned one circular grid, the focal point is lowered (with a vertical distance defined as the layer pitch) and the laser scans again the same area. This process is repeated multiple times for a prescribed number of layers. A design of experiments was used, in which the number of layers and the base diameter was varied as illustrated in Figure 2. The base diameter was varied from 100 µm to 400 µm in steps of 100 µm and the number of layers was varied from 150 to 600 in steps of 150. The hatch pitch and layer pitch were fixed at 15 µm and 2 µm, respectively. For each set of parameters, micro cavities were created in an array of 3 x 3 with a distance between the centre points equal to two times its base diameter.

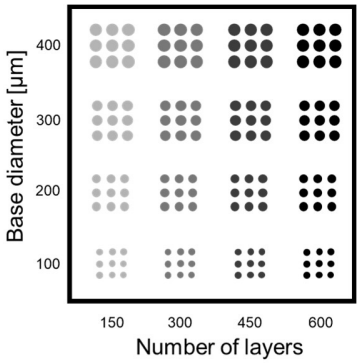


**Figure 2** Illustration of the design of laser experiments, in which the number of layers and the base diameter was varied.

### *2.3 Replication through injection moulding*

The injection moulded part selected for this study is a 50 mm x 60 mm x 1.5 mm flat plate, as shown in Figure 3. The polymer is injected through a hot runner which is located 3 mm from the edge of the product, indicated by a white dot. The array of micro needles is 12 mm x 12 mm in size, located 10 mm from the edge of the plate.

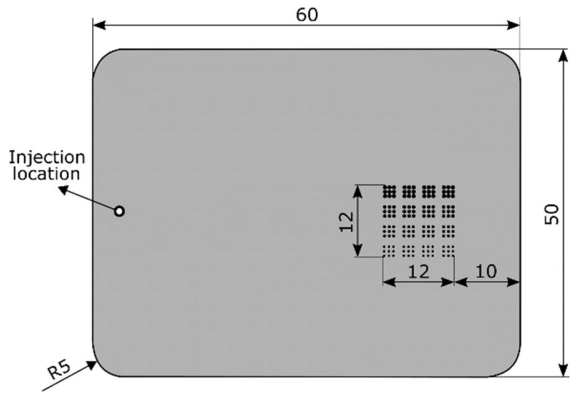


**Figure 3** Illustration of the flat plate with all dimensions in mm, the thickness is 1.5 mm.

The injection moulding machine used for this study is an Engel ES 200/35 HL hydraulic injection moulding machine with a maximum clamping force of 350 kN and a 25 mm horizontal screw with an L/D ratio of 24.8. The temperature of the mould is controlled by a Wittmann Tempro D controller. Injection moulding parameters are given in Table 3 and were defined to achieve a high replication fidelity. The injection temperature was set to the recommended upper limit of the material supplier. The mould temperature was set to a high value to delay the formation of the frozen layer during injection. The

volumetric injection rate was set to a high value, to increase shear stresses and thus reduce the melt viscosity during injection. The implemented holding pressure was set to a value just below the occurrence of flash.

**Table 3** Injection moulding process parameters for the two thermoplastic materials.

| | PC | PP |
|---|---|---|
| Injection temperature (°C) | 315 | 240 |
| Volumetric injection rate (cm³/s) | 149 | 149 |
| Holding pressure (bar) | 749 | 575 |
| Mould temperature (°C) | 115 | 80 |

The stationary side of the injection mould was equipped with a temperature sensor (Priamus, 4008B) and a piezoelectric pressure sensor (Priamus, 6001B), which allows for precise process control and online measurement of the apparent viscosity. This viscosity measurement is a build-in module in the Priamus FILLCONTROL and is, as described by [22], based on the following Equation:

$$\eta = \frac{\Delta P \cdot \Delta t \cdot H^2}{12 \cdot S} \tag{1}$$

where $\eta$ is the apparent viscosity, $\Delta P$ the pressure increase when the polymer reaches the temperature sensor, $\Delta t$ the time required for the polymer melt to flow from the pressure sensor to the temperature sensor, *H* the height of the mould cavity, and *S* the distance between the pressure and temperature sensor. The height of the mould cavity is 1.5 mm and the distance between the sensors is 100 mm. The online apparent viscosity is measured for 10 different volumetric injection rates, ranging from 15 cm³/s to 147 cm³/s.

### *2.4 Topography characterization*

The geometries of the ablated microneedle cavities were characterized using a Phoenix Nanotom micro-computed tomography (µ-CT) system. The device is equipped with a high-power nanofocus X-ray tube and a diamond-tungsten target was chosen for the high X-ray absorbing metal samples. A high-power mode was used to allow focal spot and voxel sizes in the micrometre range. A set of mould inserts, identical to those used in the injection moulding process, were cut down in cubic samples with an edge length of approximately 3 mm, using a metallographic precision saw. The samples were mounted on a

sample holder and fixed on a high-accuracy computer controlled rotation stage. For each scan, 2400 X-ray 2D projection images were obtained from incremental rotation of the scanned samples over 360°. Acquisition parameters were fixed for all samples as follows: voltage = 100 kV, current = 158 µA, voxel size = 3.75 µm, and a 0.1 mm copper and 0.1 mm aluminium filter were used during scanning. Reconstruction of the acquired 2D projections into 3D volumes was performed using GE Phoenix datos|x REC software. Reconstructed XY datasets (slices) were exported from the software in 16-bit tiff format for further analysis and visualization within Fiji ImageJ. Before conducting measurements, the Nanotom instrument was calibrated using a calibration rod (Goekeler Messtechnik, VTX18CE000-022) with an uncertainty of 1.0 µm. For each set of laser parameters, one cubic sample containing nine micro holes was measured. The average length and diameter of these nine holes along with a 95 % confidence interval, using the Student's t distribution was reported in the plotted results.

The geometries of the replicated thermoplastic microneedles were assessed using a digital microscope (Keyence VH-S30) with a maximum magnification of X200. The system is connected to a VHX-500F monitor with built-in measuring software. The microscope was calibrated using a stage micrometre (Olympus Tokyo, OBMM 1/100) which has an uncertainty of 0.5 µm. Nine samples were injection moulded and on each sample one microneedle was measured for each set of micro holes. The average of these nine measurements along with a 95 % confidence interval, using the Student's t distribution was reported in the plotted results.

### *2.5 Contact angle measurements of polymer melts*

A Dataphysics OCA 15 plus, equipped with a Dataphysics TEC 350 temperature control unit was used to measure contact angles of molten thermoplastic materials on the different mould surfaces. The equipment utilizes electric heating elements which make it possible to heat up the measurement chamber from 40 °C to 350 °C. The temperature within the chamber is measured and controlled through a thermocouple close to the polymer melt. Square samples of 15 mm x 15 mm were cut out of the different mould materials and were all grinded and polished to a roughness of $Ra < 0.1$ µm. The measurement starts by placing a polished mould substrate in the chamber for 8 min in order to heat it up evenly. A thermoplastic granule cut in half is then placed on the mould substrate. In order to minimize the initial surface contact, the granule is placed on the substrate with the spherical side facing down, as described by Bex et al. [23]. The measurement was started when the contact angle of the thermoplastic reached a value of 135 °C, as at this angle the granulates formed a drop-like shape for

each thermoplastic. Thereafter, the contact angles are registered every 30 s for a total of 20 min. The measurements were carried out under a nitrogen environment to prevent the oxidative degradation of the polymer melt and the oxidation of the metal substrates. The testing temperature of the chamber was set to the processing temperature of the corresponding thermoplastic. For each thermoplastic material, this procedure is repeated three times. The average of these three measurements, along with the 95 % confidence interval Student's t distribution are plotted versus time.

## 3 Results and discussion

### *3.1 Diameter of the micro cavities*

The effects of the number of layers in regards to the obtained cavity diameters at the surface of the mould inserts were evaluated for the three mould materials as depicted in Figure 4. First of all, we can observe small error-bars, indicating a good repeatability. In fact, the highest relative standard deviation for tool steel, copper alloy, and aluminium corresponds to 3.8 %, 3.7 % and 3.4 %, respectively. This indicates a high repeatability of the laser process, in relation to the ablated base diameter. Secondly, the cavity diameter at the mould surface created with 150 layers are in all cases lower than the programmed diameters. This interesting result can be allocated to negative dynamic effects of the optical beam deflector system. This optical beam deflector system is a key component in laser micro machining platforms that consists of reflective mirrors mounted on highly precise galvanometer motors [24]. The system realises the computer controlled movements of the laser beam along a predefined machining path. Within these machining paths, there will be regions of acceleration and deceleration at the start and end of each machining vector, which will induce a discrepancy between the programmed and the actual beam movements [25]. State-of-the-art beam deflection systems try to compensate these negative dynamic effects by introducing scanner and laser delays which give more time to the mirror galvanometers to complete their programmed movements and adjust the triggering of the laser-on and laser-off delays, respectively [26]. These delays should be optimised for different processing speeds and different machining geometry paths [27]. It can be assumed that this optimisation was not seamless, which resulted in smaller hole diameters at the surface of the mould, compared to the programmed circles. Thirdly, it can be observed that the cavity diameter at the mould surface increases with higher numbers of layers, for all of the investigated mould materials. As the amount of layers increases, the vertical position the focal spot moves deeper inside the material. Therefore, the Gaussian shaped laser beam will start to intersect with the edge of the already created micro-hole. If the power density in this intersecting region of the Gaussian beam is higher than the ablation threshold, additional material will be removed. Thus, as a result of a higher numbers of layers, the diameter of the micro-hole at the surface of the mould insert will increase. At last, it can be observed that there is a difference in the hole dimensions between the investigated materials. This discrepancy will be further discussed in section 3.2.

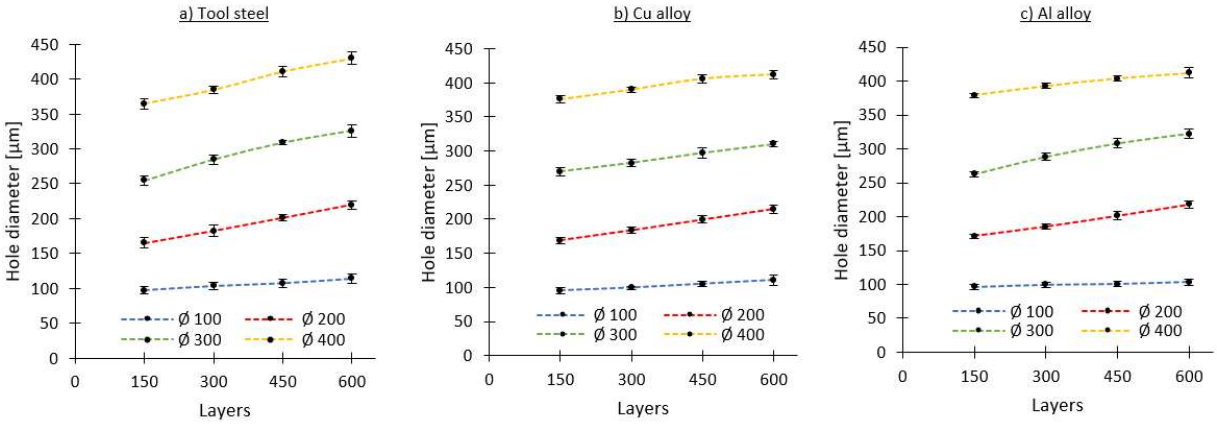


**Figure 4** Micro cavity diameter at the surface of the mould insert in function of varying number of layers for different programmed diameters for following materials: (a) tool steel, (b) copper alloy, and (c) aluminium alloy. The error bars represent the 95 % confidence interval.

### *3.2 Formation of the cone-shaped micro cavities*

The effects of the laser parameters in regards to the micro cavities were investigated for the three different mould materials. Here, the number of layers and the programmed base diameter were both varied in four different levels and the micro cavities produced with each of these settings were analysed by the cross sectional views obtained from the µ-CT measurements, as shown in Figure 5. Cone-shaped micro-holes with very low tip radii are observed for all sets of laser parameters and mould materials. The formation of the cone-shape is expected to be a result of two phenomena: (i) a plasma shielding effect and (ii) laser reflectance on a micro-hole with a steep sidewall. This first phenomenon occurs during laser ablation processes with high repetition rates (> 5 kHz) [28]. During such processes, solid material is ablated into vaporised material. This vapour is partially ejected from the micro cavity, yet the other part remains near the surface, held by surface energies. When the laser repetition rate is low (< 5 kHz), the time interval between each pulse is large enough for the vapour to escape the micro cavity or to ensure the formation of a recast layer [29]. At higher repetition rates > 5 kHz, the time interval between pulses is reduced to < 200 µs, which causes an interaction between the vaporised material and the incoming pulse, forming a plasma. This plasma absorbs and defocuses the laser beam, creating a protective shield called “plasma shielding effect” [30]. The deeper the ablated micro-hole, the more difficult the vaporised material can escape the hole, which in turn increases the protective shield [31]. The second phenomenon is laser reflectance on a micro-hole with a steep sidewall. When ablating such

micro-holes, the steep sidewalls will reflect most of the laser light rather than absorb it. Therefore the ablation efficiency near the edge of the cavity is reduced, causing the diameter to become smaller as the micro-hole is created [32]. In addition, the reflected laser light will partially be redirected to the bottom of the hole, possibly contributing to a deeper and sharper cavity. Thus, due to both phenomena, cone-shaped micro-holes are created using the presented laser strategy.

Although cone-shaped micro-holes are observed for all of the investigated mould materials, the cavity shape and dimensions differ between the materials, yet the same machining strategy and laser parameters were used. This is due to differences in material properties, such as absorptivity, heat capacity, thermal conductivity, and electron–phonon coupling constant [33]. The thermal conductivity has an influence on the re-solidification of the material melt. A low thermal conductivity leads to a high re-solidification time [34]. Hence, the laser pulses will irradiate on a melt surface which reacts like a liquid dielectric [35,36]. This fluid state requires much higher pulse energy to be ablated, thus the lower thermal conductivity results in a decrease in ablation efficiency. This theory was also confirmed by Cheng et al. [28] who found that the solidification of the melt layer for Al and Cu, both metals with a high thermal conductivity, was very fast, which improved the ablation efficiency. The electron-phonon interaction is another material parameter that influences the ablation rate. This interaction occurs when a laser pulse strikes a metal surface causing electrons in the material to excite through photon absorption. The excited electrons will equilibrate with the surrounding lattice though electron-phonon coupling. The time required for electron-phonon equilibration is proportional to the electron-phonon coupling constant [12]. A high electron-phonon coupling constant results in rapid energy transfer between the electrons and the solid lattice, which in turn leads to a lower electron diffusion depth [13]. Consequently, a high electron-phonon coupling constant causes a large fraction of the laser energy to be retained close to the incident surface, leading to a rapid rise in surface temperature which enhances the ablation efficiency. Researchers determined the electron-phonon coupling constants for 316L stainless steel [37], pure aluminium [38], and pure copper [39–41] through pump-probe experiments and the corresponding values are presented in Table 4. Although these materials are not identical to the tool steel, aluminium alloy, and copper alloy used in this study, we assume the coupling constants to be within the same order of magnitude as the corresponding material. Thus, using these values, we have an indication of the thermal conductivity (Table 2) and the electron-phonon coupling constants (Table 4) for our materials, which we will link to the obtained micro-holes through femtosecond laser ablation.

The depth of the micro-holes produced in the aluminium alloy are significantly lower compared to the micro-holes made in tool steel and copper. This is due to its low electron-phonon coupling constant relative to the high coupling constant of the tool steel. Besides, the thermal conductivity is lower compared to the copper alloy. The micro-holes for the tool steel and copper alloy are quite similar, which can be allocated to the high electron-phonon coupling constant and high thermal conductivity respectively. These findings confirm that surface ablation via femtosecond laser irradiation is more favourable on metals with a high electron–phonon coupling constant and a high thermal conductivity.

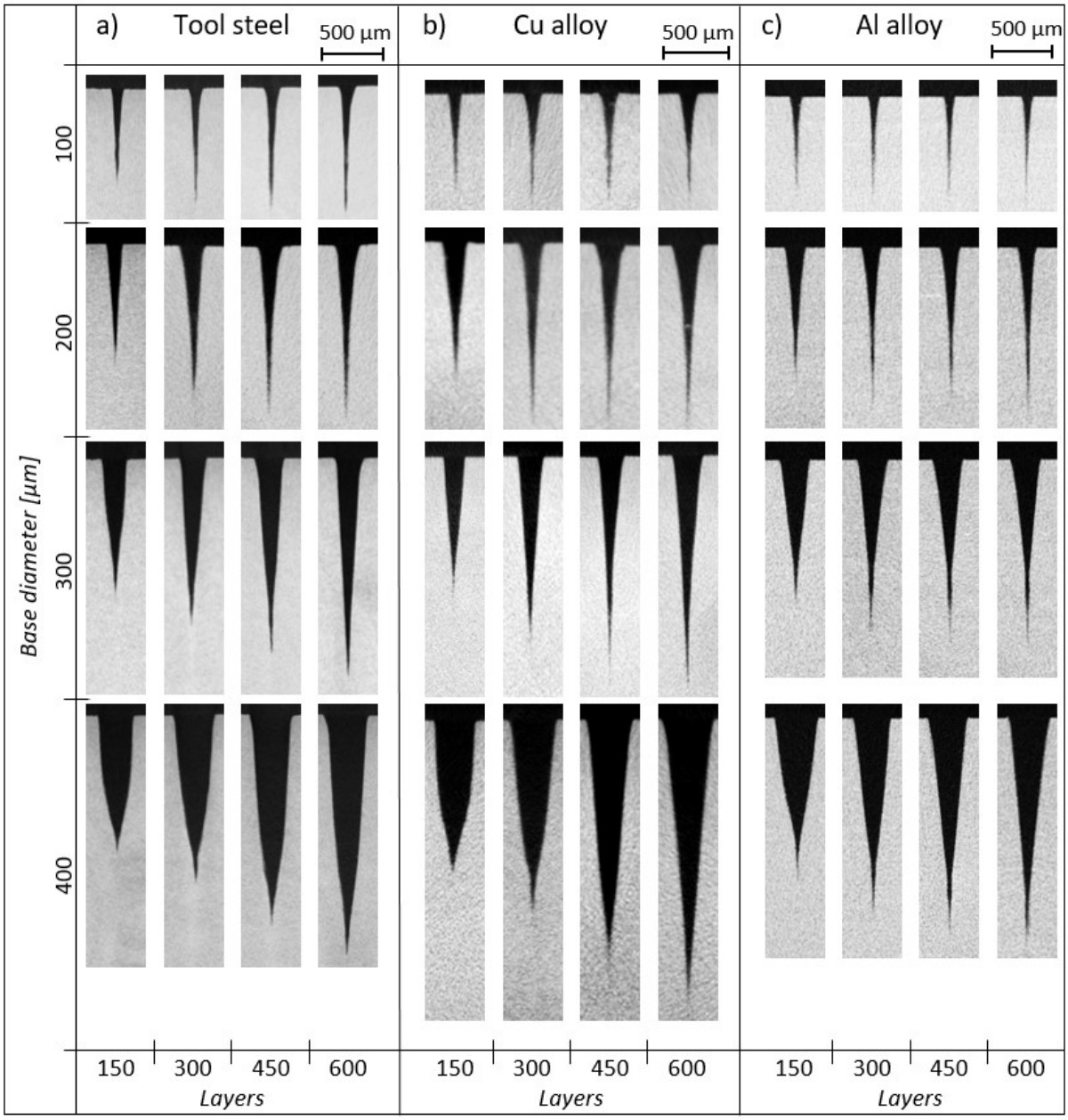


**Figure 5** Cross sectional views obtained from the µ-CT measurements of the micro-holes created with the design of laser experiments for following materials: (a) tool steel, (b) copper alloy, and (c) aluminium alloy. A scale bar is included for each of the materials.

**Table 4** Electron-phonon coupling constants for stainless steel 316L, aluminium and copper.

| | Electron-phonon coupling constant ($10^{17}$ W $m^{-3}$ $K^{-1}$) |
|---|---|
| Stainless steel 316L | 54 [37] |
| Aluminium | 2.45 [38] |
| Copper | 1 [39] ; 0.45 [40,41] |

### *3.3 Depth of the micro cavities*

The produced micro cavities were analysed by measuring the hole depth in the cross sectional views obtained from the µ-CT measurements. The hole depth for the different programmed hole diameters in function of the number of layers is shown in Figure 6. First of all, all of the error bars are similar. The average confidence interval is approximately 27 µm, indicating a very high repeatability of the ablation process. Consequently, the smaller micro cavities have a higher relative error compared to the large cavities. This could be due to measurement errors, as in the needle tip area, the size approaches the measured voxel size of 3.75 µm.

Secondly, for the holes produced with a programmed diameter of Ø400 mm and Ø300 mm it can be seen that with an increase in the number of layers, the depth of the micro holes increases. This can easily be explained by an increase of accumulated fluence, as the number of layers is increased. However, for the holes produced with a programmed diameter of Ø200 mm and Ø100 mm, the increase in depth decreases as the number of layers is increased. In other words, there is a saturation in the depth after a certain number of layers. The smaller the programmed hole diameter, the faster the saturation point is reached. For the holes with a larger diameter, it can be assumed that there will also be a saturation point. However, this saturation was not yet reached within the investigated number of layers. The occurrence of saturation is already known for laser percussion drilling (repeatedly pulsing focused laser energy on one spot) [32,42]. Within our laser strategy the saturation could be explained as follows: as an ablated hole gets deeper, the diameter of the hole decreases and the walls become steeper, therefore, the reflection and surface area of the wall increase, causing a drop in the absorbed energy density [43]. Consequently, less energy will be absorbed by the bottom of the cavity, creating a saturation depth after a certain number of layers.

Thirdly, when looking at Figure 6, a relation can be observed between the depth of the cavities and the programmed base diameters. As the programmed base diameter increases for a constant number of layers, the micro cavities become deeper. As already explained in section 3.2, the diameters of the micro holes increase with a higher number of layers. Moreover, we known that the micro holes have conical shapes in which the diameter keeps decreasing throughout the depth of the hole until the diameter becomes very small and forms the tip radius of the hole. When starting with a large base diameter, the amount of layers required to reach this very small tip radius will be larger, compared to a hole with a small base diameter. Thus, deeper holes can be created when starting with a larger base diameter. Moreover, when starting with a small base diameter, the fraction of laser energy that will be reflected near the edge of the hole will be relatively high compared to the total emitted laser energy. Thus, only a part of the laser energy will be utilised for the ablation process, resulting in holes with a lower depth. Holes with a large base diameter will be able to utilise a larger fraction of the emitted laser energy for the ablation process, resulting in a higher accumulated fluence and thus deeper micro cavities.

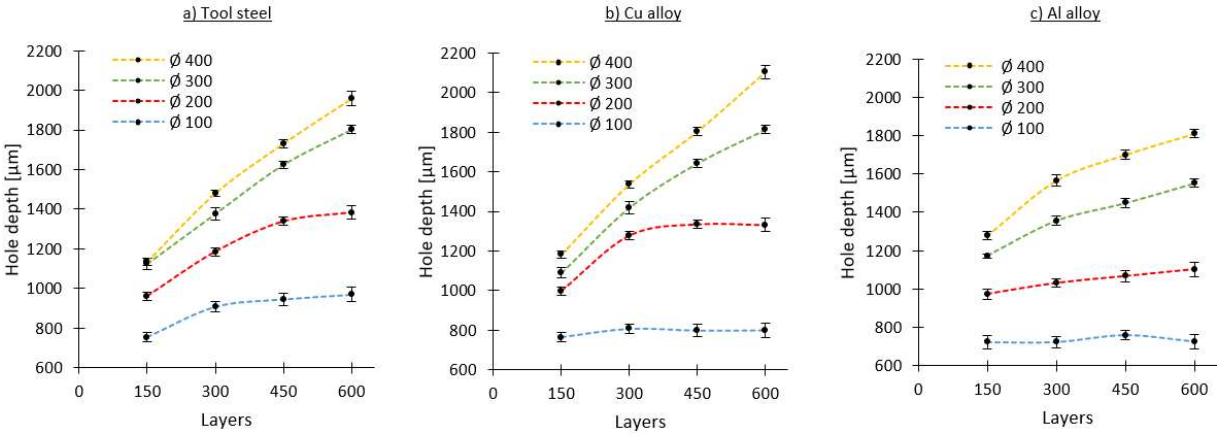


**Figure 6** Hole depth in function of the programmed hole diameter for varying number of layers for following materials: (a) tool steel, (b) copper alloy, and (c) aluminium alloy. The error bars represent the 95 % confidence interval.

### *3.4 Replication through polymer injection moulding*

The mould inserts with laser ablated microneedle cavities are used in the injection moulding process to create polymer microneedles, both in PP and PC. A microscopic image of a PP plate replicated with an aluminium insert is shown in Figure 7 (a), which illustrates the 16 microneedle arrays with different dimensions. Figure 7 (b) shows a representation of a polypropylene microneedle fitted into the corresponding aluminium microneedle cavity created with a diameter of 400 µm and 300 layers. The tip radius of the microneedle corresponds to the hole radius at the depth of the microneedle.

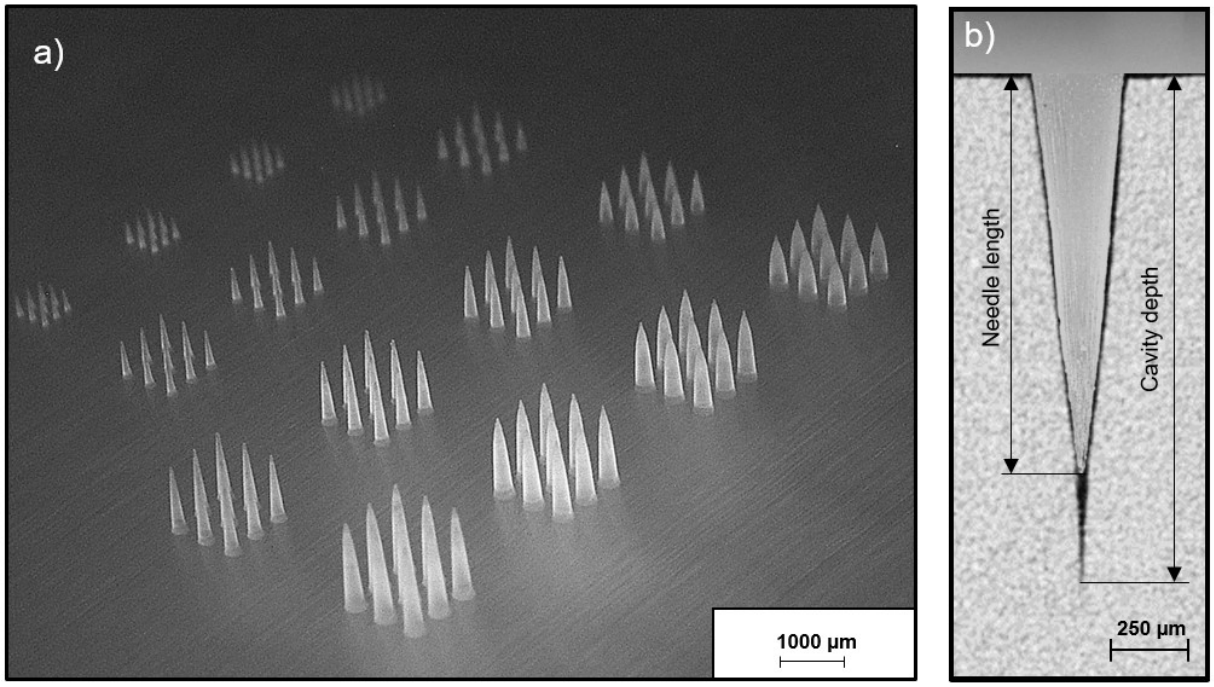


**Figure 7** (a) Microscopic image of a polypropylene plate replicated with an aluminium mould insert. (b) Representation of a polypropylene microneedle fitted in the corresponding aluminium microneedle cavity created with a diameter of 400 µm and 300 layers.

During the injection moulding, the polymer melt fills the cavity and is then packed and cooled inside the microneedle mould cavities. This results in a change in specific volume of the polymer melt during a moulding cycle. At the end of the cooling stage, the specific volume has decreased, which corresponds to a volumetric shrinkage of the polymer. The volumetric shrinkage can be determined using the compressibility (or PVT) behaviour of the polymer. This can be modelled by the double domain Tait equations, which specify the specific volume as a function of melt pressure and temperature [19]. The PVT plots and corresponding double domain Tait coefficients of the selected polymers are shown in

Figure 8. A reasonably accurate estimate of the volumetric shrinkage can be calculated if the polymer, pressure and temperature at the end of the packing stage are known. We assume the pressure at the end of the packing stage to be equal to the holding pressure and the temperature to be equal to the no-flow temperature. First, the specific volume ($v$) is modelled as a function of pressure and temperature as:

$$v(T,P) = v_0 \cdot \left[1 - 0.0894 \cdot \ln\left(1 + \frac{P}{\beta}\right)\right] + v_T \tag{2}$$

where $v_0$ is the reference specific volume, P the pressure, $\beta$ the compressibility and $v_T$ represents the additional specific volume associated with the transition of semi-crystalline polymers. The ratio of the specific volumes $r_v$ is calculated as a function of the specific volume of the plastic at the end of the packing stage $v(T_{no\_flow}, P_{pack})$ and the specific volume of the plastic during end use of the moulded part $v(T_{end\_use}, P_{end\_use})$.

$$r_v = \frac{v(T_{no\_flow}, P_{pack})}{v(T_{end\_use}, P_{end\_use})} \tag{3}$$

Eventually, by assuming the polymer to be isotropic, the linear shrinkage s can be calculated as:

$$s = 1 - \sqrt[3]{r_v} \tag{4}$$

Using the no-flow temperatures corresponding to Table 1, a room temperature of 20 °C, and holding pressures listed in Table 3, a linear shrinkage of 0.43 % and 2.22 % are found for PC and PP, respectively. These values correspond to typical values found in literature for amorphous and semi-crystalline polymers. Thus, both microneedles will undergo a shrinkage, which is approximately 5 times higher for PP compared to PC.

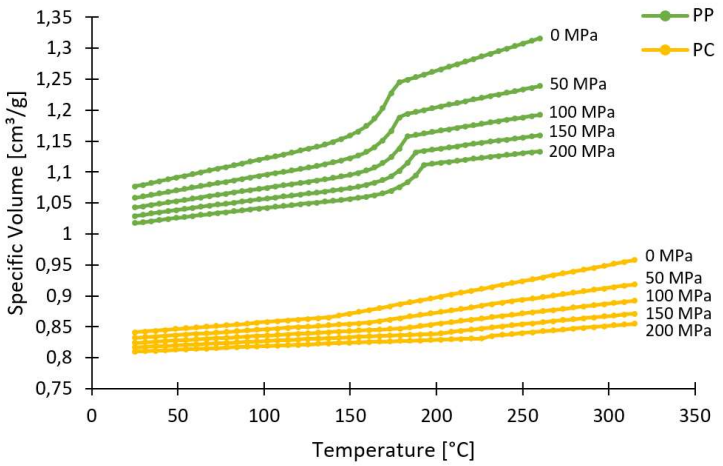


**Figure 8** PVT plots of PC and PP, based on the Autodesk Moldflow® 2019 material database.

The replication of the needles is assessed by comparing the height of each needle to the depth of the corresponding micro cavity. Thus, the replication of the needles is represented as a filling percentage in height, which also includes shrinkage. The replication of the PC and PP microneedles in height, relative to the aspect ratio of the holes in each of the mould materials is presented in Figure 9. The standard deviation for the replication in height is on average 15 µm for all of the replications. This shows that the injection moulding process has a very high repeatability, in terms of replication. Within each graph, a linear function ($y_{Steel}$, $y_{Cu}$, $y_{Al}$) together with its correlation coefficient (R) is expressed between the replication in height and the aspect ratio of the holes for each of the mould materials. For both thermoplastics, a clear linear relationship between the replication in height and the aspect ratio of the holes can be observed. The higher the aspect ratio of the hole, the lower the replication of the microneedle. This relationship is caused by two phenomena. First, during the initial filling stage the polymer will follow the path of least resistance. Therefore, most of the material will flow in the main flow direction through the macro-scale cavity, leaving the micro features only partially filled, also known as the hesitation effect [44]. These micro features will then only be filled after the rest of the cavity is filled and the pressure rises. Second, with an increase in aspect ratio, the surface area to volume ratio increases, which results in higher heat transfer between the molten polymer and the mould surface [45]. This results in a faster solidification of the polymer. Thus due to the hesitation effect the micro cavity is only partially filled during the initial filling stage. In addition, when the macro cavity is filled and the pressure is built up, the polymer is already solidified due to the higher heat transfer. Therefore, microneedle cavities with a high aspect ratio result in a lower replication.

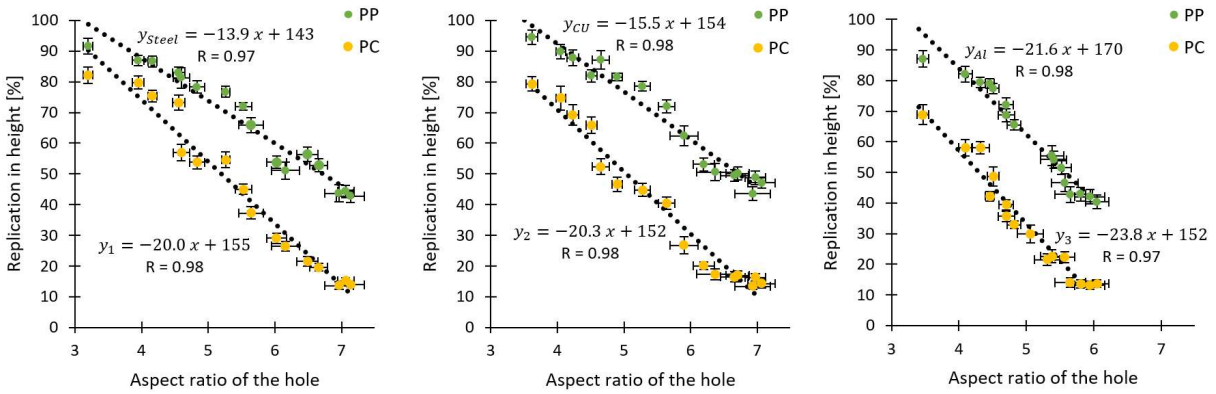


**Figure 9** Replication of the PP and PC microneedles in height, relative to the aspect ratio of the holes in (a) tool steel, (b) copper alloy and (c) aluminium alloy. The vertical error bars represent the combined 95 % confidence interval of the hole depth and the replicated microneedle; the horizontal error bars represent the combined 95 % confidence interval of the hole depth and the hole diameter.

### *3.5 Difference in replication between the mould materials*

In Figure 9 we can distinguish differences in replication between the three mould materials. The replication in height is, as already discussed, related to the aspect ratio of the corresponding micro hole.

The replication of the PP microneedles at a low aspect ratio is similar for the three mould materials. Nonetheless, there is a significant difference in the slope of the linear functions. The slope is the lowest for tool steel, closely followed by the copper alloy, and the highest for the aluminium alloy. For the PC microneedles, it can be observed that the slopes are much steeper compared to PP, meaning the replication decreases faster for an increase in aspect ratio. In addition, the PC microneedles moulded in the aluminium alloy insert have a lower replication at low aspect ratios, compared to tool steel and copper alloy. Similar to PP, the slopes of the linear functions are lower for the tool steel and the copper alloy, and higher for the aluminium alloy. This indicates that the replication of the microneedles with tool steel and copper alloy are comparable, while being much higher compared to the aluminium alloy.

The discrepancy in filling between the three materials is expected to be a result of differences in thermal and wetting properties. Lucchetta et al. [46] investigated the influence of the thermal diffusivity of the mould material on the replication fidelity within injection moulding. It was found that a mould material with low thermal diffusivity could improve the replication of features with high aspect ratios. This effect is related to the ability of the mould material being able to delay the formation of the skin layer during the filling. As a consequence, during the holding phase, the polymer can still be deformed to enhance the filling inside the micro cavity. However, as mentioned in section 2.3, a mould material with a lower thermal conductivity exhibits a lower ablation efficiency. In our case, the thermal diffusivity of the tool steel is a factor 10 times higher compared to the copper and aluminium alloy, as displayed in Table 2. Based on this fact alone, the tool steel would be expected to result in a better replication fidelity compared to the other two mould materials. However, the difference in thermal properties is not the only factor affecting the replication quality as wetting properties between the molten polymer and the mould surface will also play an important role [47] [48]. A better wettability between the molten thermoplastic and mould material is already known to improve the filling behaviour of micro features and this property can be characterised by contact angle measurements [49]. The results for the contact angle measurements for both polymer melts on the three different mould materials are given in Figure 10. It is clear that the wetting of PP and PC is best in combination with copper alloy, followed by

aluminium alloy and is worst for tool steel. For PP, the difference in wetting Is limited around 10° and equilibrium has not yet been reached. Also, for PC, regardless of the mould material, wetting is worse compared to PP. In terms of wetting, this indicates that the replication fidelity of the micro features should be the highest for copper alloy and the lowest for tool steel. However, as already indicated, the difference in replication between the mould materials is expected to depend on both thermal and wetting properties, in which a high thermal diffusivity and a high wetting is desirable. Tool steel has a very low thermal diffusivity, which compensates the lower wettability, while the copper alloy exhibits the highest wettability combined with a higher thermal diffusivity. The aluminium alloy however, also has a high thermal diffusivity, similar to copper combined with a weaker wettability compared to copper. This explains why the replication fidelity of tool steel and copper alloy are similar and why that of aluminium alloy is the lowest.

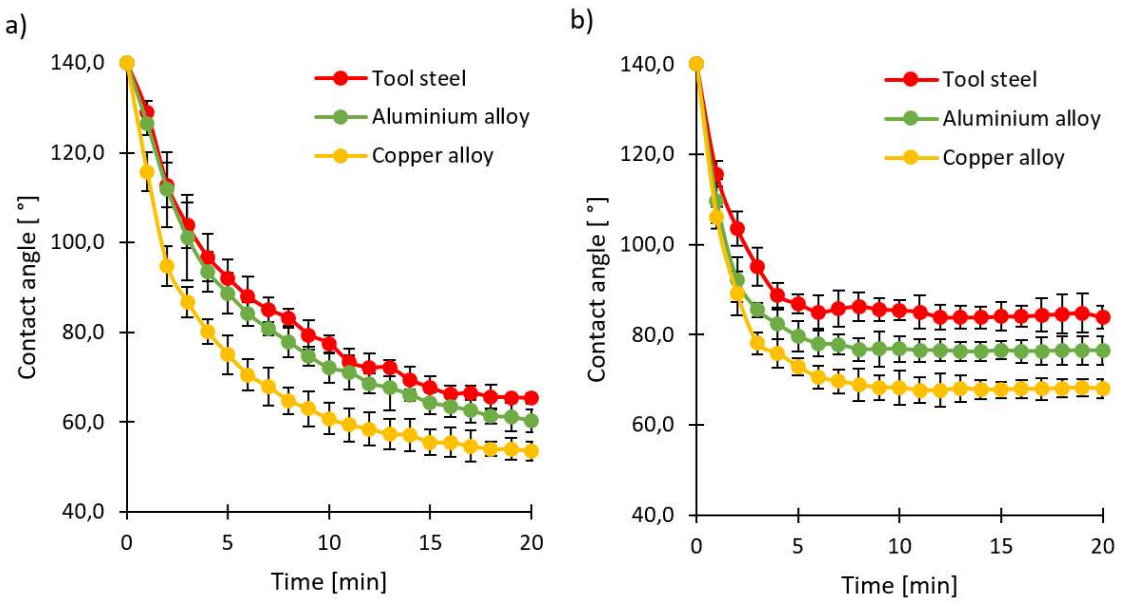


**Figure 10** Contact angle of (a) PP and (b) PC, during the spreading on the different mould materials. The error bars represent the 95 % confidence interval.

### *3.6 Difference in replication between the thermoplastics*

The difference in replication between the two thermoplastics is possibly caused by four factors.

First of all, as already discussed, there is a difference in linear shrinkage for both polymers, corresponding to 0.43 % and 2.22 % for PC and PP, respectively. Thus, the PC microneedles will only exhibit a very low linear shrinkage in the orders of a few micrometres, while the PP will have a linear shrinkage in the orders of a few tens of micrometres.

Secondly, the large surface area to volume ratio of the microneedle cavities, makes interfacial phenomena such as wettability critical. In fact, during the very early contact between the polymer melt and the mould, before the skin formation, the wetting at the interface between the polymer melt and the mould plays an important role in the filling of the micro features. Rytka et al. [47] and Vera et al. [48] observed that a higher work of adhesion (or spreading coefficient) between the polymer melt and the mould results in a better filling of the micro features. Vera et al. [48] determined a work of adhesion on a steel substrate of 42.8 mJ/m² for PP and 30.0 mJ/m² for PC, which corresponded to a better micro replication of PP compared to PC. Although the PP and PC grades and the steel used in the work of Rytka et al. [47] are not identical to our grades, we expect the interfacial wetting behaviour to be comparable.

The third factor inducing a discrepancy in replication is the different creep deformation behaviour of the two materials. Creep deformation has been reported in literature as an important variable with respect to the replication of small features [50,51]. During the packing phase, the polymer skin layer has to undergo a deformation in order to further enhance the replication of the features beyond the level reached during the initial filling. This deformation is only possible if the temperature of the skin layer is still higher than the no-flow temperature, which is the temperature when a polymer ceases to flow. The time, t, required for the average temperature of the polymer to reach the no-flow temperature, $T_{nf}$ ,can be estimated using Eq. (5), as presented in [52].

$$t = \frac{a^2}{\pi^2 \cdot \alpha} \cdot ln\left[\frac{8}{\pi^2} \cdot \left(\frac{T_i - T_m}{T_{nf} - T_m}\right)\right] \quad (5)$$

with $a$ the thickness of the polymer part, $\alpha$ the thermal diffusivity ,$T_i$ the injection temperature, and $T_m$ the mould temperature. Using this equation and the data from Table 1, on average the times required for PP and PC to reach the no-flow temperature are 8.9 s and 4.8 s, respectively. These values will be

much higher than the time required for the skin layer to reach the no-flow temperature. However, we can clearly observe a large difference between both polymers, as the time required for the PP sample to reach the no-flow temperature is nearly two times higher than for the PC sample. This will result in a much faster solidification of the PC skin layer compared to PP. In fact, it is possible that at the start of the packing phase, the skin layer of the PC sample is already frozen and is unable to be deformed whereas the PP skin layer is still able to deform.

The fourth parameter inducing the difference in filling between both thermoplastics is the melt viscosity. This viscosity decreases with an increasing shear rate, also known as shear thinning. This effect is caused by the disentanglement of the polymer chains, which align along the direction of shear. Higher shear rates decrease the melt viscosity, which improves the filling of small micro cavities. When filling the microneedle cavities, two different orders of shear rates can be distinguished: (i) very high shear rate during the injection phase, which partially fills the microneedle cavities, and (ii) a very low shear rate during the packing phase, which further enhances the filling. The melt viscosity during the injection phase can be determined from Cross-WLF (Cross–Williams–Landel–Ferry) rheology curves extracted from Autodesk Moldflow® and from the actual online apparent viscosity measurements. A comparison between Cross-WLF model viscosities and online apparent viscosity measurements is shown in Figure 11.

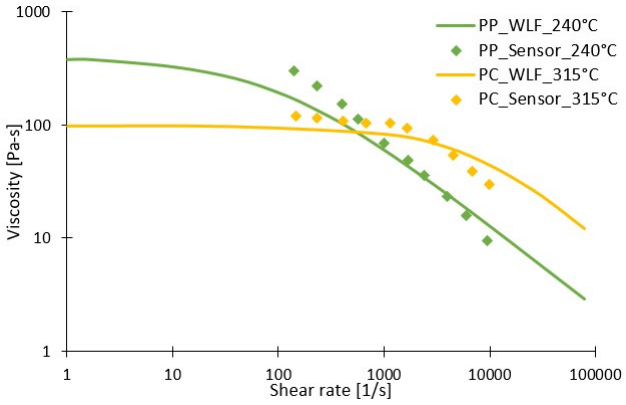


**Figure 11** Comparison between Cross-WLF model viscosities and online apparent viscosity measurements for PP and PC.

The online apparent viscosity measurements reveal higher viscosities at low shear rates and lower viscosities at high shear rates compared to the Cross-WLF model, which was also found by [53]. From

both the apparent viscosity as the Cross-WLF model viscosity, it can be seen that at very high shear rates, the viscosity of PC is higher than PP. This indicates that the micro features are more easily filled in PP during the initial filling stage at a volumetric injection rate of 149 $cm^3/s$.

### *3.7 Surface topography of the replicated microneedles*

When analysing the surface topography of the replicated microneedles, micro-grooves were observed along the entire length of the polymer needles for all of the investigated mould materials, as shown in Figure 12 (a). These grooves, being a few micrometres in width and height, are created inside the micro-holes during the laser processing and are replicated during the injection moulding process. The cause of these grooves can be allocated to the applied cross-hatching laser strategy. Because the programmed circular shape is approximated by a grid of parallel lines, the outer contour is not a homogeneous circle. In fact, the contour consists out of micro-ridges along the depth of the needle cavity. Although it is currently unknown whether the micro-grooves have a negative effect on the microneedle functionality, an adapted laser strategy is presented to avoid the formation of the grooves. In this strategy, the linear cross-hatching strategy is changed to a circular-hatching strategy as presented in Figure 12 (b). Here, the laser spot scans a circular region in concentric circles. The process conditions were identical to the cross-hatching strategy, being a steel mould insert, a hatch pitch = 15 µm, a layer pitch = 2 µm a programmed base diameter of 400 µm and the number of layers = 600. It can be observed that the needle has a similar shape and dimension compared to the needle formed with the cross-hatching strategy. However, no micro-grooves along the length of the needle were observed in the circular-hatching strategy. This is due to the fact that the outer contour is now formed by a homogeneous circle, in contrary to the cross-hatching strategy.

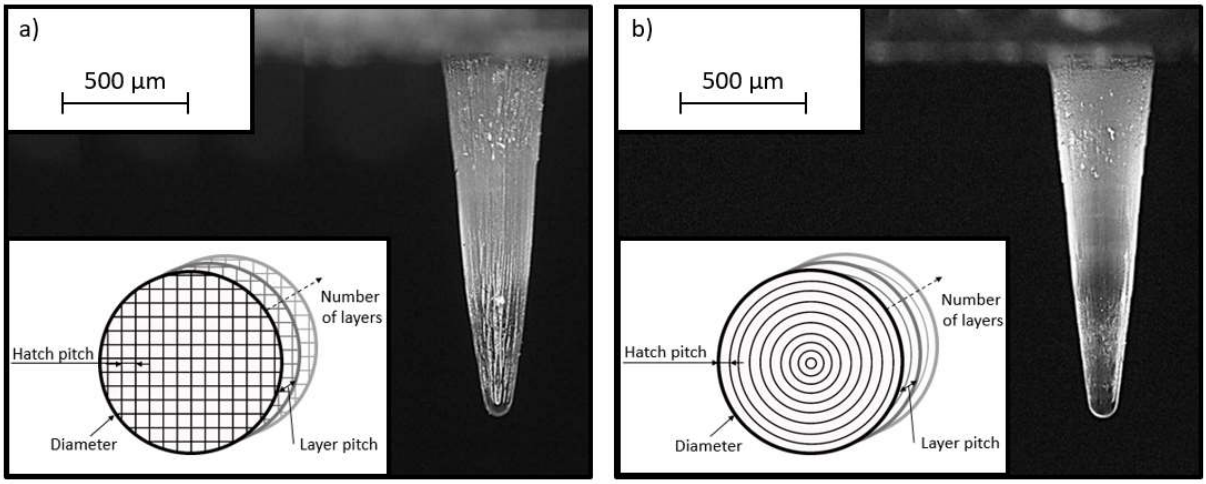


**Figure 12** Representation of a replicated PC microneedle (a) with micro grooves along the length of the needle, created with a linear cross-hatching laser strategy; (b) without micro-grooves, created with a circular-hatching strategy.

## 4 CONCLUSION

The present paper investigated the influence of two laser scanning parameters, being the programmed base diameter and the number of layers, on the geometry of microneedle cavities in tool steel, copper alloy and aluminium alloy. It was found that the depth of the micro-holes increased with a higher number of layers, due to an increase of accumulated fluence. However, there is a saturation in the increase in depth after a certain number of layers, which is reached faster for cavities with a small hole diameter. Furthermore, the replication fidelity of the laser induced cavities in these materials were evaluated for PP and PC using polymer injection moulding. A significant difference was found between the filling of PC and PP, as the replication fidelity for the PP microneedles was in all cases higher compared to the PC needles. Moreover, a linear relationship between the replication in height and the aspect ratio of the holes was found for both thermoplastics. The higher the aspect ratio of the hole, the lower the replication of the microneedle. Furthermore, a difference was identified in filling between the three different mould materials, and this could be explained by differences in thermal and wetting properties.

Thanks to this work, we better understand the effect of the investigated laser scanning parameters on the geometry of the microneedle cavities in tool steel, copper alloy, and aluminium alloy. Furthermore, a deeper insight on the effect of the aspect ratio of microneedle cavities on the replication fidelity is provided, as well as properties of polymer and mould material which affect the replication fidelity during injection moulding.

**FUNDING**

This work was supported by internal funding from KU Leuven Campus Diepenbeek, Belgium.

**ACKNOWLEDGEMENTS**

The authors would like to thank the company SABIC for providing the thermoplastic injection moulding materials.

**REFERENCES**


[1] Ita K. Transdermal delivery of drugs with microneedles—potential and challenges. Pharmaceutics 2015;7:90–105. https://doi.org/10.3390/pharmaceutics7030090.

[2] Juster H, van der Aar B, de Brouwer H. A review on microfabrication of thermoplastic polymer-based microneedle arrays. Polym Eng Sci 2019;59:877–90. https://doi.org/10.1002/pen.25078.

[3] Donnelly RF, Singh TRR, Morrow DIJ, Woolfson AD. Microneedle-mediated Transdermal and Intradermal Drug Delivery. Pondicherry: 2012.

[4] Li X (James), Zhou Y. Microfluidic devices for biomedical applications. Woodhead Publ. Ser. Biomater., Cambridge: Woodhead Publishing Limited; 2013, p. 1–652.

[5] Donnelly RF, Singh TRR, Larrañeta E, McCrudden MTC. Microneedles for Drug and Vaccine Delivery and Patient Monitoring. Chichester: 2018. https://doi.org/10.1002/9781119305101.

[6] Lee JW, Han MR, Park JH. Polymer microneedles for transdermal drug delivery. J Drug Target 2013;21:211–23. https://doi.org/10.3109/1061186X.2012.741136.

[7] Indermun S, Luttge R, Choonara YE, Kumar P, Du Toit LC, Modi G, et al. Current advances in the fabrication of microneedles for transdermal delivery. J Control Release 2014;185:130–8. https://doi.org/10.1016/j.jconrel.2014.04.052.

[8] Held J, Gaspar J, Ruther P, Hagner M, Cismak A, Heilmann A, et al. Design of experiment characterization of microneedle fabrication processes based on dry silicon etching. J Micromechanics Microengineering 2010;20. https://doi.org/10.1088/0960-1317/20/2/025024.

[9] Janphuang P, Laebua M, Sriphung C, Taweewat P, Sirichalarmkul A, Sukjantha K, et al. Polymer based microneedle patch fabricated using microinjection moulding. MATEC Web Conf 2018;192:01039. https://doi.org/10.1051/matecconf/201819201039.

[10] Yung KL, Xu Y, Kang C, Liu H, Tam KF, Ko SM, et al. Sharp tipped plastic hollow microneedle array by microinjection moulding. J Micromechanics Microengineering 2012;22. https://doi.org/10.1088/0960-1317/22/1/015016.

[11] Han M, Kim DK, Kang SH, Yoon HR, Kim BY, Lee SS, et al. Improvement in antigen-delivery using fabrication of a grooves-embedded microneedle array. Sensors Actuators, B Chem 2009;137:274–80. https://doi.org/10.1016/j.snb.2008.11.017.

[12] Yeung C, Chen S, King B, Lin H, King K, Akhtar F, et al. A 3D-printed microfluidic-enabled hollow microneedle architecture for transdermal drug delivery. Biomicrofluidics 2019;13. https://doi.org/10.1063/1.5127778.

[13] Ceyssens F, Chaudhri BP, Van Hoof C, Puers R. Fabrication process for tall, sharp, hollow, high aspect ratio polymer microneedles on a platform. J Micromechanics Microengineering 2013;23. https://doi.org/10.1088/0960-1317/23/7/075023.

[14] Kochhar JS, Quek TC, Soon WJ, Choi J, Zou S, Kang L. Effect of microneedle geometry and supporting substrate on microneedle array penetration into skin. J Pharm Sci 2013;102:4100–8. https://doi.org/10.1002/jps.23724.

[15] Larrañeta E, Lutton REM, Woolfson AD, Donnelly RF. Microneedle arrays as transdermal and intradermal drug delivery systems: Materials science, manufacture and commercial development. Mater Sci Eng R Reports 2016;104:1–32. https://doi.org/10.1016/j.mser.2016.03.001.

[16] Urdea M, Penny LA, Olmsted SS, Giovanni MY, Kaspar P, Shepherd A, et al. Requirements for high impact diagnostics in the developing world. Nature 2006;444 Suppl 1:73–9. https://doi.org/10.1038/nature05448.

[17] Attia UM, Marson S, Alcock JR. Micro-injection moulding of polymer microfluidic devices. Microfluid Nanofluidics 2009;7:1–28. https://doi.org/10.1007/s10404-009-0421-x.

[18] Evens T, Malek O, Castagne S, Seveno D, Van Bael A. A novel method for producing solid polymer microneedles using laser ablated moulds in an injection moulding process. Manuf Lett 2020;24:29–32. https://doi.org/10.1016/j.mfglet.2020.03.009.

[19] Kazmer DO. Injection Mold Design Engineering. München: Carl Hanser Verlag GmbH & Co. KG; 2007. https://doi.org/10.3139/9783446434196.

[20] Prashanth Reddy K, Panitapu B. High thermal conductivity mould insert materials for cooling time reduction in thermoplastic injection moulds. Mater Today Proc 2017;4:519–26. https://doi.org/10.1016/j.matpr.2017.01.052.

[21] Altenberger I, Kuhn HA, Müller HR, Mhaede M, Gholami-Kermanshahi M, Wagner L. Material properties of high-strength beryllium-free copper alloys. Int J Mater Prod Technol 2015;50:124–46. https://doi.org/10.1504/IJMPT.2015.067820.

[22] Sykutera D, Czyzewski P, Kocęciuszko A, Szewczykowski P, Wajer L, Bieliński M. Monitoring of the injection and holding phases by using a modular injection mold. J Polym Eng 2018;38:63–71. https://doi.org/10.1515/polyeng-2016-0321.

[23] Bex GJ, Seveno D, De Keyzer J, Desplentere F, Van Bael A. Wetting measurements as a tool to predict the thermoplastic/thermoset rubber compatibility in two-component injection molding. J Appl Polym Sci 2018;135. https://doi.org/10.1002/app.46046.

[24] Engelmayer A. Galvanometer scanning speeds laser processing. Ind Laser Solut 2005:9–11.

[25] Penchev P, Dimov S, Bhaduri D, Soo SL, Crickboom B. Generic software tool for counteracting the dynamics effects of optical beam delivery systems. Proc Inst Mech Eng Part B J Eng Manuf 2017;231:48–64. https://doi.org/10.1177/0954405414565379.

[26] Buls S, Craeghs T, Clijsters S, Kempen K, Swevers J, Kruth JP. The influence of a dynamically optimized galvano based laser scanner on the total scan time of SLM parts. 24th Int SFF Symp - An Addit Manuf Conf SFF 2013 2013:260–6.

[27] Mirtchev T, Weeks R, Minko S. Optimizing the feedback control of Galvo scanners for laser manufacturing systems. Photonics North 2010 2010;7750:77500T. https://doi.org/10.1117/12.873068.

[28] Cheng J, Perrie W, Edwardson SP, Fearon E, Dearden G, Watkins KG. Effects of laser operating parameters on metals micromachining with ultrafast lasers. Appl Surf Sci 2009;256:1514–20. https://doi.org/10.1016/j.apsusc.2009.09.013.

[29] Petkov P, Scholz S, Dimov S. Strategies for material removal in laser milling. Conf. Multi-Material

Micro Manuf., vol. 3, 2008.

[30] Bulgakov A V, Bulgakova NM. Thermal model of pulsed laser ablation under the conditions of formation and heating of a radiation-absorbing plasma. Quantum Electron 1999;29:433–7. https://doi.org/10.1070/QE1999v029n05ABEH001503.

[31] Markopoulos AP, Koralli P, Kyriakakis G, Kompitsas M, Manolakos DE. Molecular dynamics simulation of material removal with the use of laser beam. Mater. Form. Mach., Elsevier; 2016, p. 117–53. https://doi.org/10.1016/C2013-0-16282-4.

[32] Audouard E, Mottay E. Engineering model for ultrafast laser microprocessing. Front Ultrafast Opt Biomed Sci Ind Appl XVI 2016;9740:974016. https://doi.org/https://doi.org/10.1088/0022-3727/34/18/327.

[33] Bharatish A, Soundarapandian S. Influence of Femtosecond Laser Parameters and Environment on Surface Texture Characteristics of Metals and Non-Metals – State of the Art. Lasers Manuf Mater Process 2018;5:143–67. https://doi.org/10.1007/s40516-018-0059-1.

[34] von Allmen M, Blatter A. Laser-Beam Interactions with Materials. vol. 2. Berlin, Heidelberg: Springer Berlin Heidelberg; 1995. https://doi.org/10.1007/978-3-642-57813-7.

[35] Song KH, Xu X. Explosive phase transformation in excimer laser ablation. Appl Surf Sci 1998;127–129:111–6. https://doi.org/10.1016/S0169-4332(97)00619-3.

[36] Nedialkov NN, Atanasov PA, Breitling D, Heusel G, Dausinger F. Ablation of metals by ultrashort laser pulses. In: Atanasov PA, Gateva S V., Avramov LA, Serafetinides AA, editors. Proc. SPIE, vol. 5830, 2005, p. 80–4. https://doi.org/10.1117/12.617375.

[37] Bévillon E, Colombier JP, Dutta B, Stoian R. Ab initio nonequilibrium thermodynamic and transport properties of ultrafast laser irradiated 316l stainless steel. J Phys Chem C 2015;119:11438–46. https://doi.org/10.1021/acs.jpcc.5b02085.

[38] Hostetler JL, Smith AN, Czajkowsky DM, Norris PM. Measurement of the electron-phonon coupling factor dependence on film thickness and grain size in Au, Cr, and Al. Appl Opt 1999;38:3614. https://doi.org/10.1364/ao.38.003614.

[39] Elsayed-Ali HE, Norris TB, Pessot MA, Mourou GA. Time-resolved observation of electron-phonon relaxation in copper. Phys Rev Lett 1987;58:1212–5. https://doi.org/10.1103/PhysRevLett.58.1212.

[40] Qiu TQ, Tien CL. Short-pulse laser heating on metals. Int J Heat Mass Transf 1992;35:719–26. https://doi.org/10.1016/0017-9310(92)90131-B.

[41] Brorson SD, Kazeroonian A, Moodera JS, Face DW, Cheng TK, Ippen EP, et al. Femtosecond room-temperature measurement of the electron-phonon coupling constant in metallic superconductors. Phys Rev Lett 1990;64:2172–5. https://doi.org/10.1103/PhysRevLett.64.2172.

[42] Nasrollahi V, Penchev P, Jwad T, Dimov S, Kim K. Drilling of micron-scale high aspect ratio holes with ultra-short pulsed lasers : Critical effects of focusing lenses and fluence on the resulting holes ' morphology. Opt Lasers Eng 2018;110:315–22. https://doi.org/10.1016/j.optlaseng.2018.04.024.

[43] Ruf A, Berger P, Dausinger F, Hügel H. Analytical investigations on geometrical influences on laser drilling. J Phys D Appl Phys 2001;34:2918–25. https://doi.org/10.1088/0022-3727/34/18/327.

[44] Yao D, Kim B. Injection molding high aspect ratio microfeatures. J Inject Molding Technol 2002;6:11–7.

[45] Hill SDJ, Kämper KP, Dasbach U, Döpper J, Erhfeld W, Kaupert M. An investigation of computer modelling for micro-injection moulding. Proc Microsym'95 1995;12:275–83.

[46] Lucchetta G, Ferraris E, Tristo G, Reynaerts D. Influence of mould thermal properties on the replication of micro parts via injection moulding. Procedia CIRP 2012;2:113–7. https://doi.org/10.1016/j.procir.2012.05.051.

[47] Rytka C, Opara N, Andersen NK, Kristiansen PM, Neyer A. On the Role of Wetting, Structure Width, and Flow Characteristics in Polymer Replication on Micro- and Nanoscale. Macromol Mater Eng 2016;301:597–609. https://doi.org/10.1002/mame.201500350.

[48] Vera J, Contraires E, Brulez AC, Larochette M, Valette S, Benayoun S. Wetting of polymer melts on coated and uncoated steel surfaces. Appl Surf Sci 2017;410:87–98.

https://doi.org/10.1016/j.apsusc.2017.02.067.

[49] Sorgato M, Masato D, Lucchetta G. Effect of vacuum venting and mold wettability on the replication of micro-structured surfaces. Microsyst Technol 2017;23:2543–52. https://doi.org/10.1007/s00542-016-3038-5.

[50] Zhang H, Fang F, Gilchrist MD, Zhang N. Filling of high aspect ratio micro features of a microfluidic flow cytometer chip using micro injection moulding. J Micromechanics Microengineering 2018;28. https://doi.org/10.1088/1361-6439/aab7bf.

[51] Baruffi F, Gülçür M, Calaon M, Romano JM, Penchev P, Dimov S, et al. Correlating nano-scale surface replication accuracy and cavity temperature in micro-injection moulding using in-line process control and high-speed thermal imaging. J Manuf Process 2019;47:367–81. https://doi.org/10.1016/j.jmapro.2019.08.017.

[52] Stelson KA. Calculating cooling times for polymer injection moulding. Proc Inst Mech Eng Part B J Eng Manuf 2003;217:709–13. https://doi.org/10.1243/095440503322011443.

[53] Rytka C, Kristiansen PM, Neyer A. Iso- and variothermal injection compression moulding of polymer micro- and nanostructures for optical and medical applications. J Micromechanics Microengineering 2015;25:1–16. https://doi.org/10.1088/0960-1317/25/6/065008.